photonics

MDPI

Article

Prediction of the Quality of Thermally Sprayed Copper Coatings on Laser-Structured CFRP Surfaces Using Hyperspectral Imaging

Jana Gebauer [1,*,†], Florian Gruber [1,†], Wilhelm Holfeld [1], Wulf Grählert [1] and Andrés Fabián Lasagni [1,2]

[1] Fraunhofer Institute for Material and Beam Technology IWS, D-01277 Dresden, Germany; florian.gruber@iws.fraunhofer.de (F.G.); wilhelm.holfeld@iws.fraunhofer.de (W.H.); wulf.graehlert@iws.fraunhofer.de (W.G.); andres_fabian.lasagni@iws.fraunhofer.de (A.F.L.)
[2] Institute for Manufacturing Technology, Technische Universität Dresden, D-01069 Dresden, Germany
* Correspondence: jana.gebauer@iws.fraunhofer.de
† These authors contributed equally to this work.

Abstract: With the progressive replacement of metallic parts by high-performance fiber-reinforced plastic (FRP) components, typical properties of metals are required to be placed on the material's surface. A metallic coating applied to the FRP surface by thermal spraying, for instance, can fulfill these requirements, including electrical conductivity. In this work, laser pre-treatments are utilized for increasing the bond strength of metallic coatings. However, due to the high-precision material removal using pulsed laser radiation, the production-related heterogeneous fiber distribution in FRP leads to variations in the structuring result and consequently to different qualities of the subsequent coating. In this study, hyperspectral imaging (HSI) technologies in conjunction with deep learning were applied to carbon fiber-reinforced plastics (CFRP) structured by nanosecond pulsed laser. HSI-based prediction models could be developed, which allow for reliable prediction, with an accuracy of around 80%, of which laser-treated areas will successfully be coated and which will not. By using this objective and automatic evaluation, it is possible to avoid large amounts of rejects before further processing the parts and also to optimize the adhesion of coatings. Spatially resolved data enables local reworking during the laser process, making it feasible for the manufacturing process to achieve zero waste.

Keywords: laser structuring; hyperspectral imaging; surface pre-treatment; coating quality prediction; machine learning; automation; metal–plastic hybrid; lightweight

Citation: Gebauer, J.; Gruber, F.; Holfeld, W.; Grählert, W.; Lasagni, A.F. Prediction of the Quality of Thermally Sprayed Copper Coatings on Laser-Structured CFRP Surfaces Using Hyperspectral Imaging. *Photonics* **2022**, *9*, 439. https://doi.org/10.3390/photonics9070439

Received: 20 May 2022
Accepted: 18 June 2022
Published: 21 June 2022

1. Introduction

The usage of fiber-reinforced plastics (FRPs) has significantly increased in the last years. This is mainly due to their favorable stiffness-to-weight ratio, making them ideal for being used in lightweight construction, including automotive and aerospace markets [1]. On the other hand, challenges must be overcome for the large-scale replacement of metal components with FRP components, including typical metal properties on the surfaces, such as those which enable wear and temperature resistance, electrical conductivity, or thermal isolation [2–4]. Therefore, to improve certain properties, a metallic coating can be applied to the FRP surface, for example, by thermal spraying [5–12]. In particular, for the case of carbon fiber-reinforced plastics (CFRP), different surface pre-treatment methods have been already investigated, such as sanding, pre-heating, etching, and even the application of additional layers. The most established surface pre-treatment method for cleaning and roughening the substrate surface is mechanical blasting [6,9,11,13,14]. Unfortunately, the highly accelerated and sharp-edged blasting particles (e.g., corundum) can damage the fibers near the surface [6]. As a result, air pockets are produced in the interface between the

FRP and the metal coating, and in these regions the long-term stability is lowered compared to an intact interface.

As an alternative, pulsed laser surface structuring methods offer a promising alternative for cleaning and roughening the CFRP surface. Smashed filaments can be prevented, no contamination occurs due to the contact free process, and no additional material is needed. Furthermore, the structuring process can be applied locally without utilizing masks, e.g., by using a laser scanner system [7,15–17]. For a good coating adhesion, a homogeneous surface quality is required. On the other hand, due to the manufacturing process, FRPs exhibit a non-uniform distribution of the reinforcing fibers. This results in an uneven amount of matrix covering the fibers. Therefore, material-specific heterogeneity cannot be compensated in all cases. Due to these inhomogeneities, it is conceivable that using identical laser parameters will yield different results concerning the surface topography depending on the matrix layer thickness above the carbon fibers. For instance, some areas of the FRP material can show after the laser treatment the exposure of the reinforcing fibers while in other regions the fibers can be still covered by the epoxy matrix. This is in particular the case when pre-treating different batches of the FRP material. Therefore, it might be necessary to adjust the operating laser parameters (especially the laser power) during the process to ensure consistent adhesion strengths of the coating. Until now, the laser-treated FRP must be subjected to optical inspection, whether visually or by means of a microscope. The qualitative evaluation is subject to the objective assessment of the processor and thus depends on his or her experience [18–21].

To overcome these issues, an in-line process monitoring concept, e.g., using hyperspectral imaging (HSI), could be used to control the quality of the laser structuring results as well as predicting the coating adhesion of the coating layer. In consequence, areas requiring additional treatment could be identified even during the structuring process.

HSI method has shown to enable rapid spatial and spectral analysis of surfaces. In a hyperspectral measurement, a complete spectrum in the wavelength range under investigation is obtained for each point on the measured sample surface. The result is called a hypercube. The wavelength range is not limited to the visible part of the spectrum, but can be extended into the ultraviolet, the near-infrared, and the mid-infrared. It is also possible to measure Raman and fluorescence signals. Originally developed for remote sensing [22], HSI has now found uses in many other applications, such as in agriculture, recycling, medicine, and pharmaceuticals [23–26]. The analysis of hyperspectral data is mostly done using machine learning [27], and recently increasingly also using deep learning, i.e., convolutional neural networks (CNN). Paoletti et al. [28] provided a comprehensive review of the current state-of-the-art methods for HSI classification, analyzing, and correlation of imaging data. Machine learning for the evaluation of hyperspectral data is used, for example, for agricultural and medical applications [29,30]. For the prediction of adhesion properties of coatings using hyperspectral data and machine learning, there are currently very few publications [31].

In this article, it is investigated whether it is possible to predict the coating adhesion of a thermal sprayed Cu layer on laser-processed CFRP components using hyperspectral imaging and deep learning methods. For this purpose, CFRP samples are pre-treated with three different surface qualities and characterized using two different HSI systems. The copper-deposited areas are correlated with the recorded image data and used to train, optimize, and validate U-Net CNNs [32] to predict the coating adhesion.

2. Materials and Methods

2.1. Materials

CFRP parts (SIGRAPREG® C U-600-0/SD-E501/33%) with a thickness of 2 mm consisting of an epoxy resin were used in this study. The fiber volume content is specified as 67% with unidirectional oriented carbon fibers (from SGL Carbon, Wiesbaden, Germany). The structured surfaces had a rectangular geometry of 12.5 mm × 25 mm.

The coating material used was a copper wire (>99.8% Cu) with 1.6 mm diameter (from GTV Verschleißschutz GmbH, Luckenbach, Germany).

2.2. Process Chain

The first step of the process chain involved surface preparation treatment before applying the coating. Figure 1 shows schematically the complete process chain. First, the CFRP was structured using a pulsed laser beam. Afterwards, the HSI camera was used to scan the pre-treated area to detect the surface quality. Finally, the thermal spray process was applied for depositing the metal coating on the laser structured CFRP substrates. In this work, the process was performed discontinuously.

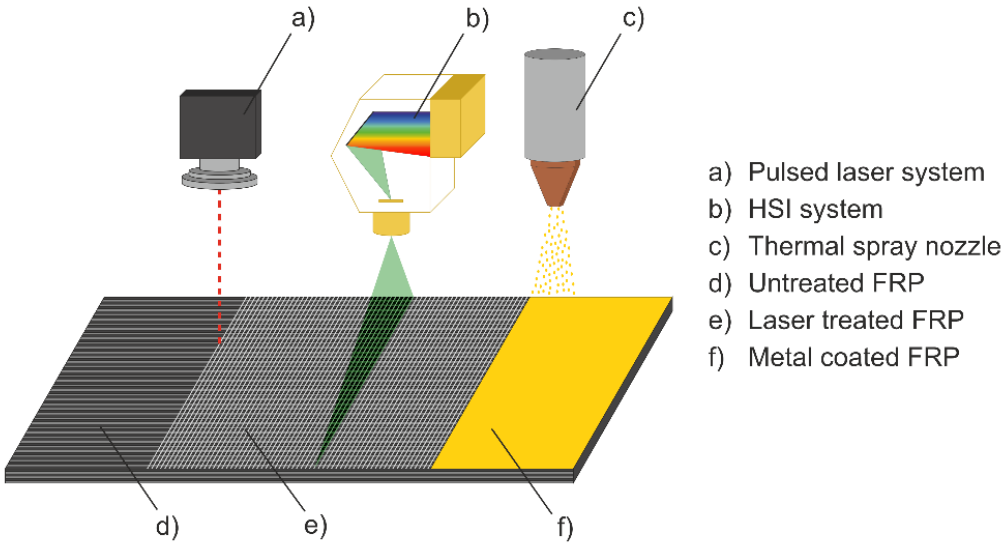

Figure 1. Process chain from untreated CFRP to laser structured surface and to coated surface including laser system, quality control by HSI system, and metallization by thermal spraying.

2.2.1. Laser Pre-Treatment Process

For the laser structuring process, a Nd:YAG laser Avia NX40 (from Coherent, Santa Clara, CA, USA) was used, offering a maximum laser power of 20 W, operating with a wavelength of 355 nm and a pulse duration of 30 ns.

For this study, a laser-roughening process is used to generate three different quality conditions in order to evaluate the monitoring method. The different quality conditions are intended to simulate the influence of different thicknesses of matrix layers above the carbon fibers and are described as follows:

- *Insufficient ablation*: carbon fibers still covered with plastic matrix.
- *Optimal ablation*: mostly exposed carbon fibers without damaged fibers.
- *Damaging ablation*: carbon fibers exposed of plastic matrix and a high amount of broken carbon fibers.

To study the influence of the amount of plastic above the fibers on the ablation pattern, it would be necessary to cover the carbon fibers with different thicknesses (in micrometer range) of homogeneous epoxy resin layers. This is not possible from a manufacturing point of view. For this reason, the following approximation must be made:

- The ablation pattern of the quality condition *insufficient ablation* can be assumed to be similar to the ablation pattern that would occur when treating a thick matrix layer.
- In contrast, it can be assumed that the ablation pattern of *damaging ablation* is similar to the ablation pattern that would occur when treating a thin matrix layer.

Details about the optical setup as well as the used laser parameters are presented in Table 1.

Table 1. Laser parameters used in this work for treating the different parts.

Quality Condition	Average Power in W	Scanning Speed in mm/s	Hatch Distance in µm	Focal Length in mm	Spot Size in µm
Insufficient ablation	1.2	1200	20	160	20
Optimal ablation	4.2[2]				
Damaging ablation	7.2[3]				

2.2.2. Thermal Spraying

The copper coating was applied using a wire arc spraying process. A spraying system consisting of the VisuArc350 inverter and the Schub5 gun (both manufactured by Oerlikon Metco Europe GmbH, Kelsterbach, Germany) was used. The gun was mounted on a robot with six adjustable axes. The operating gun was applied three times over the specimens, using a coating thickness around 100 µm [33]. The used parameters are collected in Table 2. After both the laser treatment and the coating processes, the surfaces were photographed for further evaluation. In total, 45 samples were produced.

Table 2. Thermal spraying parameters [33].

Current in A	Voltage in V	Spraying Distance in mm	Traverse Speed in m/s	Gas Pressure in MPa	Flow Rate in m^3/h
80	40	150	1	0.6	142.6

2.2.3. Hyperspectral Imaging

The hyperspectral measurements of the 45 samples produced were performed with a pushbroom HSI measuring system using either diffuse halogen (VNIR HSI) and 532 nm Nd-YAG laser illumination sources (Laser HSI). A schematic representation of the two HSI systems is shown in Figure 2. The systems are equipped with a VNIR HSI camera (Hyperspec-VNIR, Headwall Photonics Inc., Bolton, MA, USA) with a wavelength range between 400 nm and 1000 nm and a matching lens (Xenoplan 23 mm f/1.4; Jos. Schneider Optische Werke, Bad Kreuznach, Germany). The HSI camera is equipped with a CMOS detector with 1000 pixels in the spatial dimension and 1000 pixels in the spectral dimension. The sensor was 4× binned in the spectral dimension, resulting in 250 pixels covering the spectral range from 325 nm to 1111 nm.

The lighting for the VNIR HSI is provided by 6 halogen lamps with a power of 25 W each. The diffuse illumination of the samples is done by a self-designed integration tube made of optical PTFE (Spectralon, Labsphere Inc., North Sutton, NH, USA), which produces a homogeneous diffuse illumination. The lighting for the Laser HSI is provided by a 300 mW 532 nm Nd:YAG laser (GLK 32XX TS, LASOS Lasertechnik, Jena, Germany). The laser was expanded into a line by a rotating mirror (dynAxis S, Scanlab, Puchheim, Germany) and projected onto the sample by a dichroic mirror (LPD02-532RU, Semrock, Rochester, NY, USA) with an edge wavelength of 535 nm. In addition, a long-pass filter with a cut-off wavelength of 532 nm (LP03-532RE, Semrock, USA) was placed in front of the camera to block the laser light. A detailed description of the Laser HSI measurement system can be found in Gruber et al. [31]. The movement of the samples was controlled by a linear stage (VT 80, PI Micos, Eschbach, Germany) in both systems.

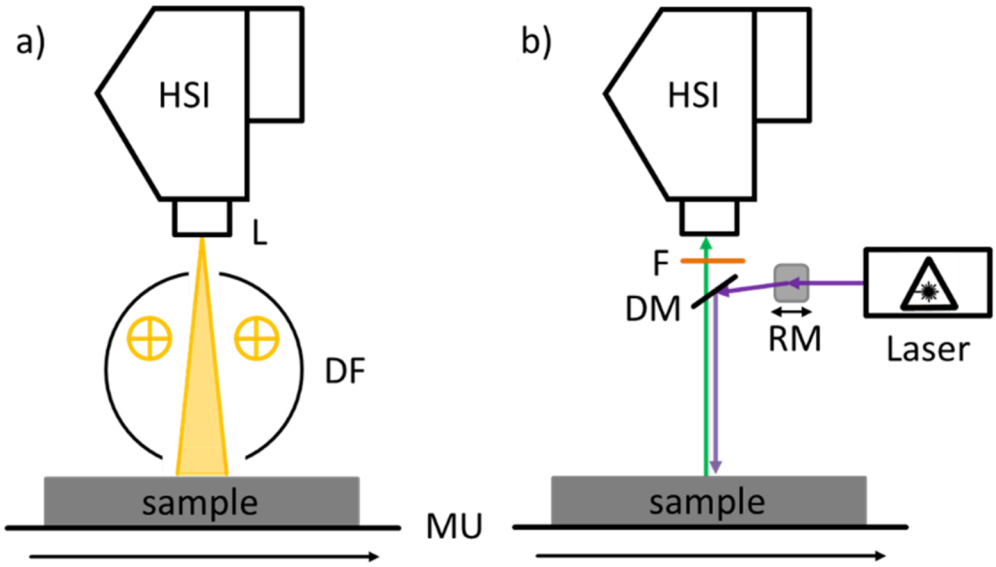

Figure 2. (**a**) Schematic representation of the VNIR HSI system and (**b**) schematic representation of the Laser HSI system. HSI: VNIR HSI camera. L: Lens. DF: Diffuse halogen illumination. F: Long pass filter. DM: Dichroic mirror. RM: Rotating mirror. MU: Motion unit.

To avoid irregularities in the lighting and to eliminate the influence of dark current, a white and a dark correction for each wavelength was carried out for the VNIR HSI measurement according to Equation (1):

$$I_c(\lambda) = \frac{I_o(\lambda) - I_d(\lambda)}{I_w(\lambda) - I_d(\lambda)} \quad (1)$$

where $I_c(\lambda)$ is the corrected image intensity for wavelength λ, $I_o(\lambda)$ is the original image intensity for the wavelength λ, $I_d(\lambda)$ is the dark current for the wavelength λ recorded with the light source switched off and the lens covered, and $I_w(\lambda)$ is the intensity for the wavelength λ of the white reference.

For the white reference, a plate of optical PTFE was scanned under the same measuring conditions as the original image. For the Laser HSI measurement, no correction was necessary.

All measurements in this work were performed at a working distance of 250 mm, resulting in a field of view (FOV) of around 100 mm and a pixel resolution of approximately 100 µm. The spectral resolution was ~3 nm. The exposure time of the camera was set to of 20 ms for the VNIR HSI measurement and to 100 ms for the Laser HSI measurement, resulting in a recording frame rate of 25 Hz and 8 Hz, respectively. The result of each measurement was a hypercube with 250 spectral bands between 325 nm to 1111 nm.

The acquisition and basic preprocessing of the hyperspectral data was done using the imanto®pro software package (Fraunhofer IWS, Dresden, Germany). It allows the control of the system components and their measurement parameters, the data acquisition, as well as the visualization and pre-processing of the acquired hyperspectral images.

2.2.4. Data Preprocessing and Analysis

The raw hyperspectral data and the images of the samples after applying the copper coatings were processed using Python version 3.9.10. Firstly, the wavelength range of the hyperspectral measurements was cut to 400 nm to 1000 nm for the VNIR HSI measurements (VNIR) and to 540 nm to 900 nm for the Laser HSI measurements (Laser). The resulting hypercubes have 191 and 142 wavelength ranges, respectively. Outside these wavelength ranges, either the quantum efficiency of the detector is too low, or no signal is expected.

Subsequently, the hyperspectral measurements as well as the photographs of the coated samples were matched. Therefore, the corner points of the samples were se-

lected manually for all measurements. The data was then converted to a uniform size of 256 × 128 pixels by projective transformation. For the hyperspectral measurements, this transformation was performed individually for each spectral channel. The images and data sets obtained are subsequently divided into smaller, non-overlapping regions with a size of 64 × 64 pixels. The binary target images for prediction are created from the photos of the samples by binarizing the red color channel with a threshold of 128. Coated areas are labeled 1 and uncoated areas are labeled 0. For training the CNNs, the target images are one-hot encoded.

Next, a principal component analysis was performed on the VNIR and laser data. For the training of the CNNs, the first five principal components were used in each case. In total, 360 hypercubes were obtained for VNIR and the laser measurements, respectively. Of these 360 hypercubes, 295 showed complete copper coating (<1% pixels detected as uncoated) and 65 showed incomplete coating. In total, around 10% of the image pixels were detected as uncoated.

2.2.5. Data Evaluation

The aim of the present work is to predict for each area of the laser-processed samples whether the thermal copper coating is successful or not. Thus, each pixel of the images is assigned a value of 0 (no coating applied) or 1 (successful coating). This is a sematic segmentation problem in which great successes have been achieved with fully convolutional neural networks (FCN) such as U-Net [32]. U-Net is an encoder-decoder structure, which means that the encoder extracts features from the input data by convolution and continuously reduces the size of the input data through pooling. Through multi-scale feature fusion and up-sampling, the decoder then generates a segmented image with the same size as the input. In this work, a modified U-Net is used, which implements residual connections according to Cholet et al. [34] in addition to the classical U-Net structure. In the following paragraphs, the structure, training, and optimization of the used U-Net are described.

An image with size $n \times 64 \times 64$ is input into the neural network. The number of channels n was 5 for the data sets, since the first five score values of the PCA of the hypercubes are used. The final output image of the neural network has a size of $2 \times 64 \times 64$. Each pixel position corresponds to a two-dimensional vector indicating if the copper coating will be successful or not.

The encoder arm of the network corresponds to a conventional CNN: unpadded convolutions (Conv2D) are applied repeatedly, each followed by a rectified linear unit (ReLU), a batch normalization layer (BatchNorm), and a 2×2 max pooling with a stride of 2 for down-sampling. In the decoder arm, an up-sampling of the feature maps is followed by a convolution, followed by ReLU and BatchNorm layers. In addition, it is possible to combine the features from the encoder arm with the up-sampled features from the decoder arm (concatenate) [32]. Furthermore, there are so called residual connections where a 1×1 convolution with stride of 2 is used. The feature maps from the residual layer are then merged with the feature maps from the normal convolution (resid) [34]. The final layer maps the feature maps to the two target classes.

The best architecture for each data set is determined by an automatic hyperparameter optimization using the Hyperband Tuner of the Keras library [35] in a separate optimization experiment using a validation data set. The optimized hyperparameters here are the number of filters for the convolutional layers (f), the number of down/up-sampling steps (m), the kernel size of the convolutional layers, whether there is a concatenate connection between the encoder and the decoder arm of the U-Net (concatenate), and whether a residual layer is used (resid).

The training of the U-Nets is done with the Python library Keras [36] on a workstation with an Intel i7 8700k CPU, 32 GB RAM and an Nvidia Geforce GTX1080 GPU. The hyperspectral measurements were pre-processed as described in chapter 2.2.4, and 30 of the 360 training samples were randomly selected as validation and test set, respectively. The training was repeated five times with a different split of training, validation, and test set.

For the training of the CNNs the RMSprop algorithm [37,38] was used and categorical cross entropy was chosen as the loss. The learning rate was set to 0.001 and reduced by a factor of 0.2 if no reduction in the loss on the validation data was achieved after 25 epochs. In total, the training was performed for 250 epochs.

The models obtained were evaluated using the test set with the indicators balanced accuracy, mean intersection over union (IoU), precision (P), recall (R), and the F1 score. Precision P and recall R can be defined as follows:

$$P = \frac{TP}{TP + FP} \tag{2}$$

$$R = \frac{TP}{TP + FN} \tag{3}$$

where TP, FP, and FN are the true positive, false positive, and false negative pixels, respectively. F1 is defined basing on the harmonic mean of precision and recall:

$$F1 = \frac{2 \cdot P \cdot R}{P + R} \tag{4}$$

Later, the balanced accuracy is defined as:

$$\text{balanced accuracy} = \frac{1}{2}\left(\frac{TP}{TP + FN} + \frac{TN}{FP + TN}\right) \tag{5}$$

The successfully coated pixels are considered as positive instances. Finally, the mean IoU describes the overlap between the areas predicted to be successfully copper-coated and the areas actually successfully copper-coated and is calculated as:

$$\text{mean IoU} = \frac{TP}{TP + FP + FN} \tag{6}$$

2.2.6. Optical Characterization Method

The surface of the laser-treated surfaces were investigated with the light microscope VHX-5000 (from Keyence, Osaka, Japan).

3. Results and Discussion

3.1. Laser Structuring Treatment

The uneven distribution of the reinforcing fibers due to production is shown in the cross section in Figure 3a. In addition, Figure 3b shows a representative ablation result after the pulsed laser process. From these images, it can be seen that while surface near fibers became exposed from matrix material (*optimal ablation* in the central region in Figure 3b), the epoxy resin is still covering the deeper carbon fibers (*insufficient ablation* on the right in Figure 3b). In those areas where the carbon fibers are covered by a larger amount of plastic than in other areas, *insufficient ablation* occurs locally, highlighted in Figure 3b. In consequence, local reworking within this component may be necessary to prevent local defects in the metal coating.

As mentioned in Section 2.2.1, different surface qualities have been produced in this work for evaluating adhesion of thermally sprayed copper coatings deposited on laser textured surfaces. These were produced using the process parameters described in Table 1.

As it can be seen in Figure 4, in case of *insufficient ablation* (Figure 4a) the topography is characterized by a high amount of matrix. The carbon fibers are still covered by remaining epoxy because the polymer matrix was only partly ablated. An *optimal ablation* (Figure 4b) is given, by a heterogeneous surface structure. A small amount of matrix residues (reflective, white areas in Figure 4b) remained locally limited due to variations of the amount of polymer matrix above the filaments. The carbon fibers are not affected by the laser treatment. Finally, Figure 4c shows the *damaging ablation* condition, characterized by a

homogeneous structure without matrix residues. The surface shows a high amount of damaged carbon fibers, visible in Figure 4c by shadowing effects along the filaments. Both, the polymer matrix and the carbon fibers were ablated during the laser process. The low surface roughness in the areas of matrix residues will lead to gaps during the coating deposition [33].

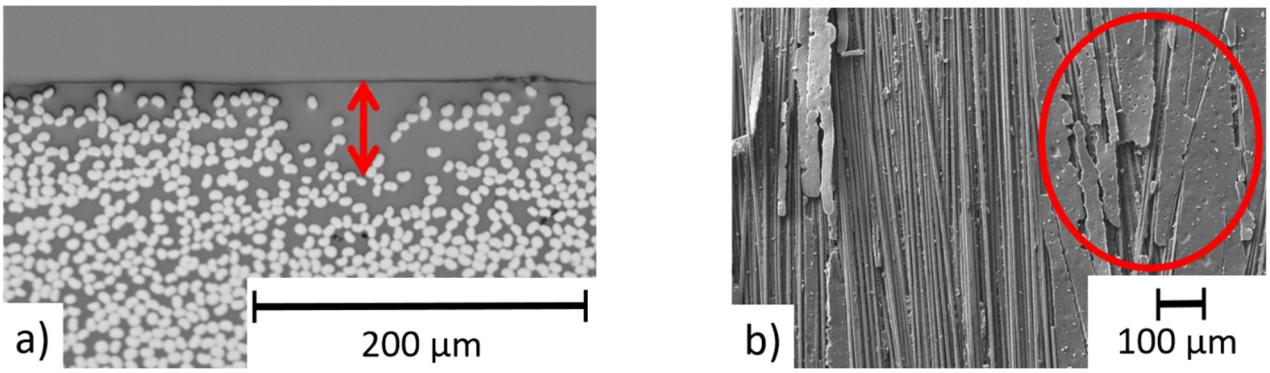

Figure 3. (**a**) Cross-section of CFRP with a highlighted area of a higher amount of epoxy resin; (**b**) heterogeneous ablation result due to heterogeneous amount of epoxy resin covering the carbon fibers, circle shows area of insufficient ablation.

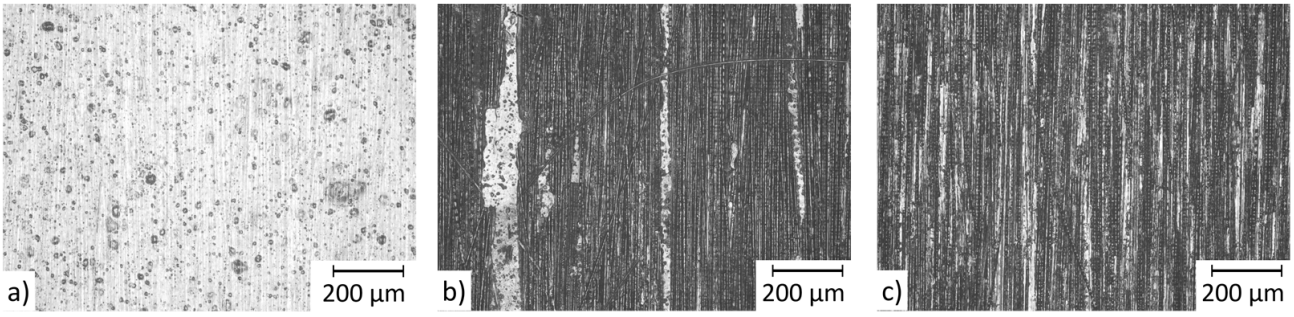

Figure 4. Optical microscope images of three surface qualities after laser pre-treatment with (**a**) insufficient, (**b**) optimal, and (**c**) damaging material removal.

With a thicker matrix layer on top of the carbon fibers (corresponding to *insufficient ablation*), the ablation of epoxy is inhibited because the removal is significantly influenced by the interaction of the laser radiation with the carbon fiber. A thick layer of plastic matrix reduces this interaction [20]. In contrast, a thinner matrix layer (corresponding to *damaging ablation*) leads to the ablation of both matrix and carbon fibers.

3.2. Coating Deposition

In Figure 5 the coating adhesions for the three surface conditions are exemplarily presented. As expected, the composite material surfaces with *insufficient ablation* led to a very heterogeneous coating adhesion (in Figure 5a,d). Areas of the specimen that appear darker in Figure 5a because the carbon fibers are locally closer to the surface, are partially covered with copper in Figure 5d. Due to the high amount of plastic residue or the low amount of exposed fibers, the substrate surface of *insufficient ablation* offers too few adhesion points for the metal particles.

On the surfaces with *optimal* and *damaging ablation* qualities, a homogeneous copper coating was obtained (in Figure 5e,f). The irregular presence of remaining matrix material (in Figure 5b) did not disable a completely coated surface due to a high amount of anchor points with the exposed carbon fibers around. Despite the broken carbon fibers on the surface of *damaging ablation* (in Figure 5c) the coating adhesion shows a completely closed copper layer similar to the specimens treated with *optimal ablation*. Consequently,

beside the surface condition with *insufficient ablation*, most specimens could be covered by copper completely.

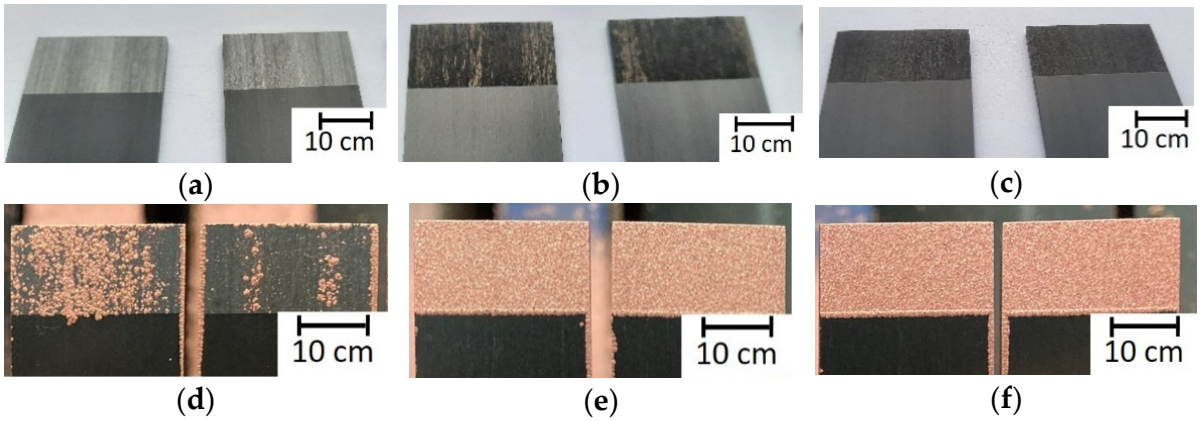

Figure 5. Optical photographs before (**a**–**c**) and after (**d**–**f**) the coating deposition treatment for CFRP surfaces with (**a**,**d**) insufficient, (**b**,**e**) optimal, and (**c**,**f**) damaging ablation conditions.

Transferred to the approximation in Section 2.2.1, this means that a thick matrix layer on top of the fibers (corresponding to *insufficient ablation*) is more critical for the coating adhesion than a comparatively thin matrix layer (corresponding to *damaging ablation*).

3.3. HSI Measurements of Laser Processed Surfaces

Figure 6 shows an example of the obtained hyperspectral measurement results of a laser processed CFRP sample. For the VNIR HSI measurement, the reflected intensity at a wavelength of 730 nm is color-coded, and for the Laser HSI measurement, the fluorescence intensity at a wavelength of 620 nm is color-coded. In addition, different spectra obtained at local positions are shown, which are indicated by colored crosses in the figure.

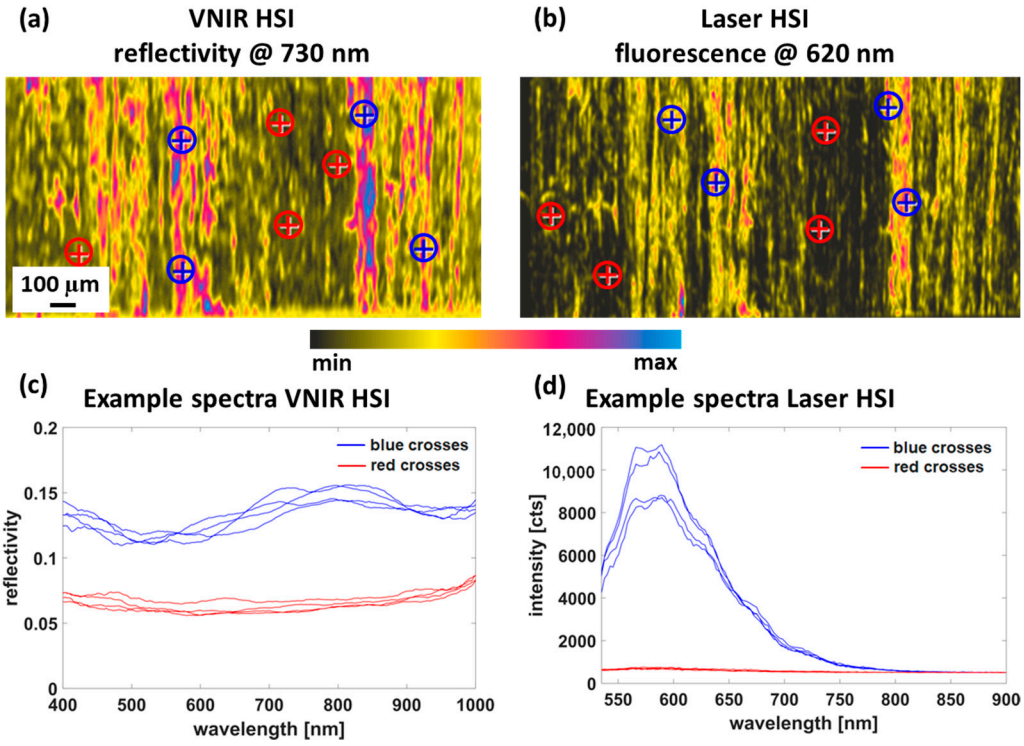

Figure 6. Examples of hyperspectral measurements for a laser processed CFRP sample. (**a**) Reflectivity (VNIR HSI) and (**b**) fluorescence (Laser HSI) at the indicated wavelength. Example spectra (**c**,**d**) of the hyperspectral measurement, the position of which is marked by colored crosses in the upper figures.

It can be seen that color-coded intensity is very similar for both measurements. Areas with high reflectivity in the VNIR measurement also show high fluorescence in the Laser HSI measurement. Based on a visual assessment of the samples and the reference measurement of non-laser processed CFRP samples, it can be assumed that the bright areas correspond to exposed or surface near carbon fibers. The matrix material, on the other hand, shows only a very weak reflection and almost no fluorescence.

In the VNIR measurement, the spectra of the exposed fiber and matrix material differ mainly in the intensity of the reflection (Figure 6a,c). The spectra of the exposed carbon fibers in the Laser HSI measurement show a strong fluorescence between 550 nm and 650 nm (see Figure 6d).

A visual comparison of the hyperspectral measurements of the CFRP specimens processed with the three different surface qualities is shown in Figure 7. The images show the color-coded reflectivities at 730 nm for the VNIR HSI measurement (Figure 7a,d,g) and the fluorescence intensity at 620 nm for the Laser HSI measurements (Figure 7b,e,h). In addition, the result of the copper coating are also shown (optical micrograph (Figure 7c,f,i)). The selected samples are characteristic for the whole set of samples.

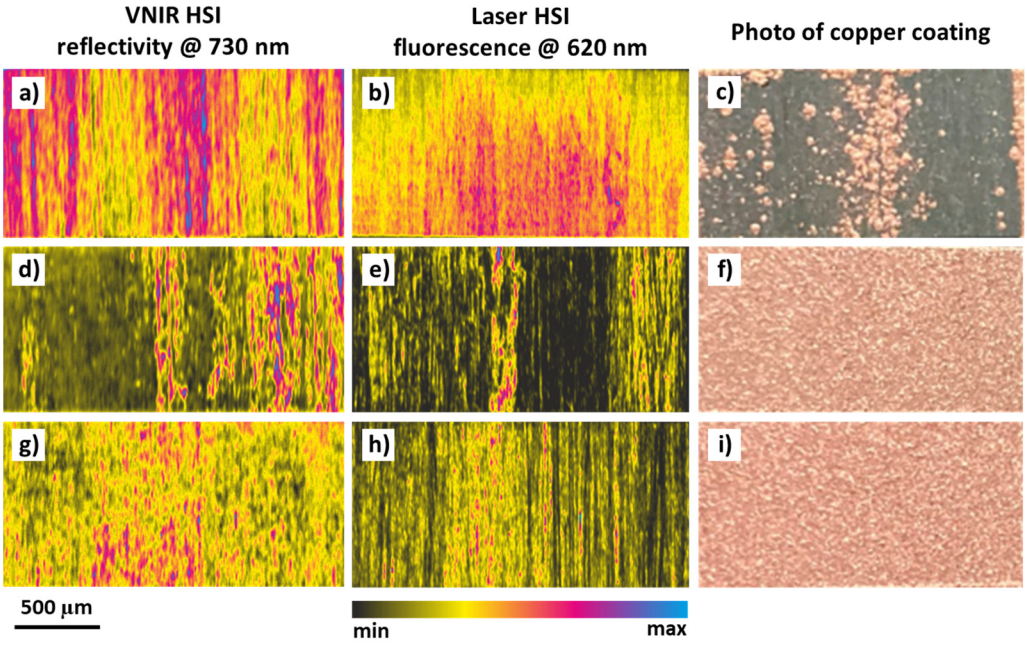

Figure 7. Comparison of hyperspectral measurements and copper coating adhesions (optical micrographs), for example, samples for each of the three sets of laser conditions used: (**a**–**c**) insufficient material removal, (**d**–**f**) optimal material removal, and (**g**–**i**) damaging material removal.

It can be seen that for the *insufficient ablation* case, only local areas of the surface were successfully coated (Figure 7a–c). For *optimal* and *damaging ablation* conditions, a good coating adhesion and uniformity of the copper coating was reached (Figure 7d–i). The hyperspectral measurements also show differences, but there is no easy recognizable link between the recorded images of the HSI measurements and the results of the copper coatings.

For the *insufficient ablation* case, a very homogeneous reflectivity for VNIR HSI and fluorescence for the Laser HSI were measured (Figure 7a–c). This can be explained by the fact that the laser structuring does not yet expose the carbon fibers and the surface is only roughened.

The surfaces with *optimal ablation* characteristics show areas with strong and weak reflectivity for the VNIR HSI and fluorescence intensity for the Laser HSI measurement, respectively (Figure 7d–f). Here, the carbon fibers near the surface are exposed to the laser radiation and can be detected very well by the HSI measurement. On the surfaces

characterized by *damaging ablation*, more areas with strong reflectivity or fluorescence intensity can be detected (Figure 7g–i). This can be attributed to a deeper exposition and the partially damaged carbon fibers.

It was also investigated whether there are differences between the spectra of the well coated and the poorly coated sample areas on average. Figure 8 shows the mean spectra of the VNIR HSI and the Laser HSI measurements for the coated and the non-coated samples. For the VNIR measurements (Figure 8a), it can be seen that the uncoated areas show a higher average reflectivity than the copper coated samples. In contrast, the coated areas show a greater variance in the recorded intensity. These results are in good agreement with the findings in Figure 7: The samples with poor copper coating adhesion have been insufficiently processed by the laser (*insufficient ablation*, Figure 7a–c) and show a relatively high and constant reflectivity. In contrast, the samples with good coating coverage (*optimal* and *damaging ablation*, Figure 7d–i) show many areas of weak reflectivity, but at the same time are very inhomogeneous due to the high reflectivity of the exposed carbon fibers.

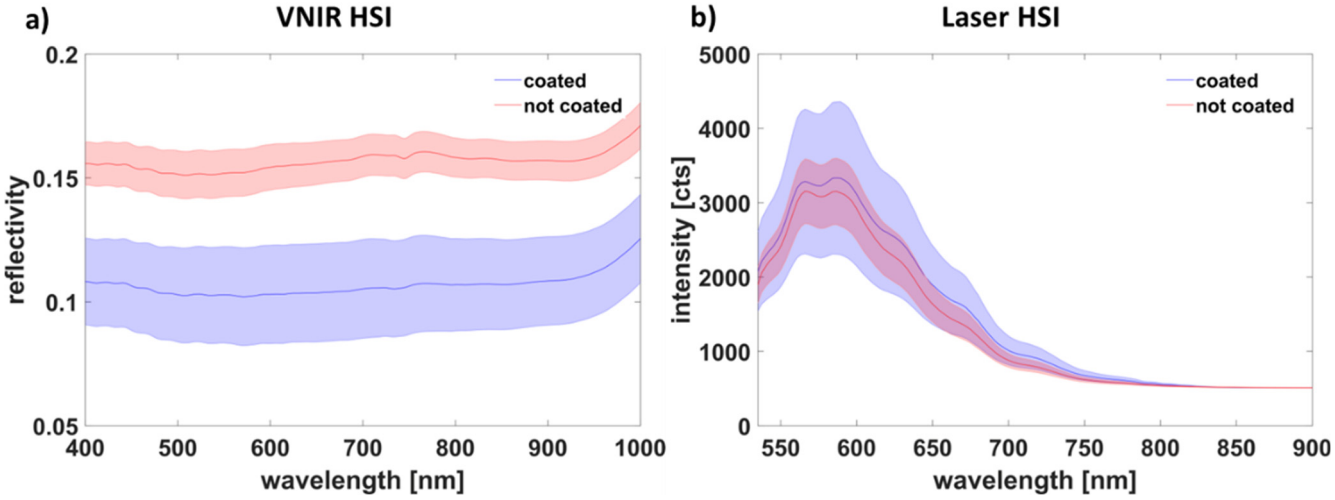

Figure 8. Averaged spectra of the (**a**) VNIR HSI and (**b**) the Laser HSI measurement for the sample areas showing a good and a bad copper coating, respectively.

These effects are not visible by the laser HSI spectra (Figure 8b). In this case, the recorded spectra show a very similar shape and intensity distributions for both materials. However, the variance is higher for the samples with good copper coating adhesion. It is likely that the fluorescence intensity is averaged out in the well-coated areas of the sample.

3.4. Data Analysis and Training

Training and hyperparameter optimization of the models were performed for the data from the VNIR and the Laser HSI measurements. The best hyperparameters found for each model are presented in Table A1 and the Appendix A. Using these parameters, complete model training was performed five times on the training data for each data set, followed by validation on the test data. The mean values and the standard deviation of the obtained quality metrics are shown in Table 3.

Table 3. Mean results and standard deviation of the metrics for predicting coating adhesion for both HSI datasets. The best value in each case is underlined. The metrics are calculated on the test data set.

Data	Precision (P)	Recall (R)	F1 Score	Balanced Accuracy	Mean Intersection over Union (IoU)
VNIR	0.954 ± 0.008	0.961 ± 0.014	0.957 ± 0.012	0.795 ± 0.031	0.880 ± 0.007
Laser	0.952 ± 0.009	0.944 ± 0.011	0.948 ± 0.009	0.784 ± 0.039	0.860 ± 0.006

The results show that the differences between the two HSI measurements are relatively small. Thus, both systems seem to provide relevant information for predicting the result of the copper coating. The best results are obtained for the VNIR measurement with a mean IoU of 0.88, a recall R of 0.961, an F1 score of 0.957, and a balanced accuracy of 0.795. The results for the laser measurement are slightly worse with a mean IoU of 0.86, a recall R of 0.944, an F1 score of 0.948, and a balanced accuracy of 0.784. Based on the calculated metrics, it appears that the best prediction results can be achieved with the VNIR measurements.

Figure 9 shows representative results of the prediction of the copper coating adhesion compared to the ground truth. Only samples for the *insufficient ablation* are presented, because for the *optimal* and *damaging ablation* conditions for both HSI measurements, the complete coating of the samples was predicted with ~100% accuracy. As it can be seen, the performed predictions are in agreement with the experimental results in all cases. For the incompletely coated samples that were pre-processed with *insufficient ablation*, the prediction of the coating adhesions for both HSI measurements is close to the ground truth, but there are deviations especially for the fine structures of the coating.

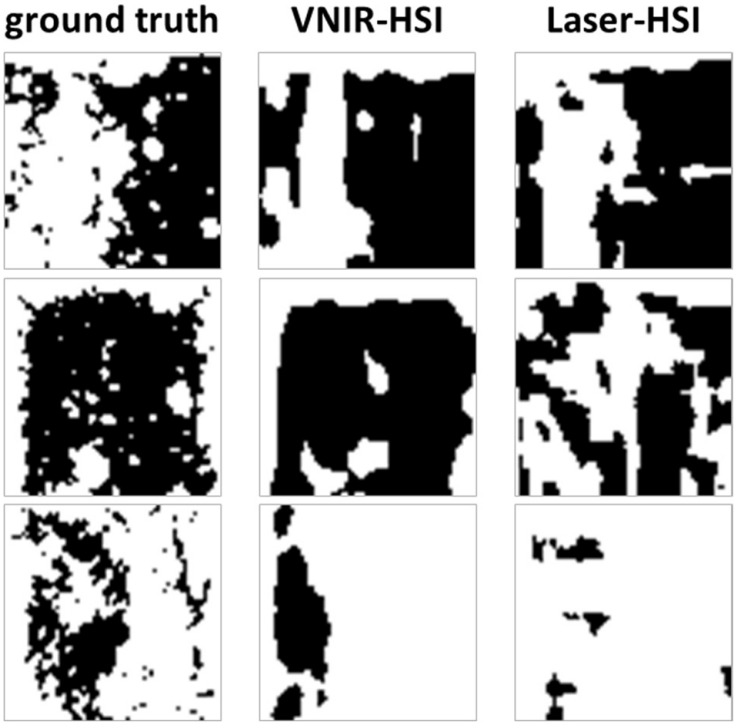

Figure 9. Ground truth and predicted copper coating for three samples from the test dataset for the two HSI methods. White pixel are copper coated and black pixels are not copper coated. The images only show samples with insufficient material removal. For the *optimal* and the *damaging ablation*, the complete copper coating was predicted correctly for both HSI methods.

Considering these results, it can be concluded that the best prediction of the success of copper coating is possible using the VNIR hyperspectral data. In addition, with both HSI methods it is possible to find areas with incomplete copper coating. The fine scaled prediction of the copper coating seems to be more challenging and is only partially successful for both HSI methods.

4. Conclusions

In this work, it was found that it is possible to predict successfully coated areas of a thermal sprayed copper layer on a laser pre-processed CFRP surface by (hyperspectral) imaging and machine learning. The results are summarized as follows:

- An objective and automatic evaluation of the surface quality of CFRP samples after laser pretreatment was developed.

- Prediction of whether a complete coating or a defective and incomplete coating will occur on the specimens is possible with high confidence.
- Prediction of successfully coated areas of a thermal sprayed copper layer are possible with an accuracy of ~80% using developed deep learning models.
- The exact spatially resolved prediction of the coating adhesion is much less accurate and only partially successful.

Based on these results, no prior knowledge of the processor is required anymore. The method developed can be used to prevent defective parts from being further processed, which would result in high reject rates. In addition, it is conceivable to use the spatially resolved data as a basis for local reworking to optimize the adhesive strengths and further minimize the reject rate or even reduce it to zero.

At the same time as the massive increase in resource efficiency due to the avoidance of rejects, the time and consequently the cost savings increase. Thus, the combination of laser technology, hyperspectral imaging, in conjunction with machine learning enables an environmentally friendly and sustainable manufacturing process. Beyond the application of thermal coating of laser-processed CFRP samples, the present study shows that hyperspectral imaging in combination with machine learning methods makes relevant and otherwise difficult-to-access surface properties obtainable, which has also been shown in other studies (see [31]). This approach opens up completely new approaches for industrial quality control.

Before the developed method can be used in industrial production, further tests beyond the scope of this feasibility study must be carried out. First, the number and variation of samples must be further increased to demonstrate the universality of the approach and to increase the robustness of the models. For example, more CFRP materials and a wider range of laser processing parameters should be investigated. In addition, the transferability of the approach from the laboratory to an industrial environment should be realized. Furthermore, it would be beneficial to investigate the causal relationship between the reflectivity or the fluorescence of the samples and the result of the copper coating. For this purpose, it would be useful to characterize the CFRP samples before and after coating using further analytical methods.

5. Patents

This work is based on the disclosures of own patents DE 10 2017 201 507 A1 and DE 10 2021 209 597.6.

Author Contributions: Conceptualization, J.G. and F.G.; methodology, J.G. and F.G.; software, W.H.; validation, J.G. and F.G.; formal analysis, J.G., W.H. and F.G.; investigation, J.G. and W.H.; resources, J.G. and W.G.; data curation, F.G.; writing and original draft preparation, J.G. and F.G.; writing, reviewing, and editing, W.G. and A.F.L.; visualization, J.G. and F.G.; supervision, A.F.L.; project administration, J.G.; funding acquisition, J.G. All authors have read and agreed to the published version of the manuscript.

Funding: This project was funded under contracts 100343527/100343532 via Sächsische Aufbaubank by the European Structural Fonds EFRE and by the Free State of Saxony. Fraunhofer Institute for Material and Beam Technology IWS Dresden funded the publication of this article.

Institutional Review Board Statement: Not applicable.

Informed Consent Statement: Not applicable.

Data Availability Statement: Not applicable.

Acknowledgments: Our project partner Chemnitz University of Technology did the process development of metal coating by wire arc spraying and performed the thermal spraying of the samples for this publication.

Conflicts of Interest: The authors declare no conflict of interest.

Appendix A

Table A1. Best found hyperparameters (see Section 2.2.5) for the U-Nets trained on the four data sets VNIR HSI (VNIR) and Laser HSI (Laser).

Hyperparameter	VNIR	Laser
Filters f	16	8
Kernel size	5	2
Down sampling steps	2	4
Concatenate	True	False
Residuen	True	True

References

1. Schürmann, H. *Konstruieren Mit Faser-Kunststoff-Verbunden*; Springer: Berlin/Heidelberg, Germany, 2007; ISBN 978-3-540-72189-5.
2. Qian, D.; Bao, L.; Takatera, M.; Kemmochi, K.; Yamanaka, A. Fiber-reinforced polymer composite materials with high specific strength and excellent solid particle erosion resistance. *Wear* **2010**, *268*, 637–642. [CrossRef]
3. Zhao, Q.; Zhang, K.; Zhu, S.; Xu, H.; Cao, D.; Zhao, L.; Zhang, R.; Yin, W. Review on the Electrical Resistance/Conductivity of Carbon Fiber Reinforced Polymer. *Appl. Sci.* **2019**, *9*, 2390. [CrossRef]
4. Martins, M.; Gomes, R.; Pina, L.; Pereira, C.; Reichmann, O.; Teti, D.; Correia, N.; Rocha, N. Highly Conductive Carbon Fiber-Reinforced Polymer Composite Electronic Box: Out-of-Autoclave Manufacturing for Space Applications. *Fibers* **2018**, *6*, 92. [CrossRef]
5. Gonzalez, R.; Ashrafizadeh, H.; Lopera, A.; Mertiny, P.; McDonald, A. A Review of Thermal Spray Metallization of Polymer-Based Structures. *J. Therm. Spray Technol.* **2016**, *25*, 897–919. [CrossRef]
6. Liu, A.; Guo, M.; Zhao, M.; Ma, H.; Hu, S. Arc sprayed erosion-resistant coating for carbon fiber reinforced polymer matrix composite substrates. *Surf. Coat. Technol.* **2006**, *200*, 3073–3077. [CrossRef]
7. Gebauer, J.; Klotzbach, U.; Lasagni, A.F. Functionalization of fiber-reinforced plastic based on laser micro structuring. In *Laser-based Micro- and Nanoprocessing XIII*; Klotzbach, U., Kling, R., Watanabe, A., Eds.; SPIE: San Francisco, CA, USA, 2019; p. 11, ISBN 9781510624542.
8. Boyer, H.; McDonald, A.; Mertiny, P. Flame Spray Deposition of Electrically Conductive Traces on Polymer Substrates for System Integrated Composite Structures. In Proceedings of the Composites 2012, Las Vegas, NV, USA, 21–23 February 2012. COMPOSITES 2012, American Composites Manufacturers Association, Ed.
9. Machulla, M.; Taghian Dehaghani, S.; Claußnitzer, P.; Scheitz, S.; McDonald, A.; Leyens, C. Thermally Sprayed Coating-Based Heating Systems for Boundary Layer Transition Detection—An Experimental Approach. In Proceedings of the International Thermal Spray Conference, Online, 24–28 May 2021; International Thermal Spray Conference. Azarmi, F., Chen, X., Cizek, J., Cojocaru, C., Jodoin, B., Koivuluoto, H., Lau, Y., Fernandez, R., Ozdemir, O., Salami Jazi, H., et al., Eds.; ASM International: Novelty, OH, USA, 2021; pp. 765–770.
10. Rezzoug, A.; Abdi, S.; Kaci, A.; Yandouzi, M. Thermal spray metallisation of carbon fibre reinforced polymer composites: Effect of top surface modification on coating adhesion and mechanical properties. *Surf. Coat. Technol.* **2018**, *333*, 13–23. [CrossRef]
11. Robitaille, F.; Yandouzi, M.; Hind, S.; Jodoin, B. Metallic coating of aerospace carbon/epoxy composites by the pulsed gas dynamic spraying process. *Surf. Coat. Technol.* **2009**, *203*, 2954–2960. [CrossRef]
12. Rezzoug, A.; Abdi, S.; Bouhelal, N.; Daoud, S. Metallic Coating for Carbon Fiber Reinforced Polymer Matrix Composite Substrate. *Int. J. Mater. Metall. Eng.* **2016**, *10*, 59–64.
13. Ganesan, A.; Yamada, M.; Fukumoto, M. The Effect of CFRP Surface Treatment on the Splat Morphology and Coating Adhesion Strength. *J. Spray Technol.* **2014**, *23*, 236–244. [CrossRef]
14. Wielage, B.; Paczkowski, G.; Mäder, T.; Rupprecht, C.; Nestler, D. Verschleißschutzschichten auf polymerbasierten Grundwerkstoffen. *Tag. Zum 18. Symp. Verb. Und Werkst.* **2011**, *41*, 646–655.
15. Heckert, A.; Zaeh, M.F. Laser Surface Pre-treatment of Aluminium for Hybrid Joints with Glass Fibre Reinforced Thermoplastics. *Phys. Procedia* **2014**, *56*, 1171–1181. [CrossRef]
16. Koshukow, W.; Krahl, M.; Gude, M.; Götz, P.; Kirchhoff, M. Influence of Laser Surface Treatment for Process-Integrated Joining of Textile Reinforced Thermoplastic Composites to Metal Sheets. In *Key Engineering Materials*; Trans Tech Publications Ltd.: Bäch, Switzerland, 2017; Volume 742, pp. 366–373. [CrossRef]
17. Gebauer, J.; Fischer, M.; Lasagni, A.F.; Kühnert, I.; Klotzbach, A. Laser structured surfaces for metal-plastic hybrid joined by injection molding. *J. Laser Appl.* **2018**, *30*, 32021. [CrossRef]
18. Akman, E.; Erdoğan, Y.; Bora, M.Ö.; Çoban, O.; Oztoprak, B.G.; Demir, A. Investigation of the differences between photochemical and photothermal laser ablation on the shear strength of CFRP/CFRP adhesive joints. *Int. J. Adhes. Adhes.* **2020**, *98*, 102548. [CrossRef]
19. Köckritz, T.; Schiefer, T.; Jansen, I.; Beyer, E. Improving the bond strength at hybrid-yarn textile thermoplastic composites for high-technology applications by laser radiation. *Int. J. Adhes. Adhes.* **2013**, *46*, 85–94. [CrossRef]

20. Gebauer, J.; Burkhardt, M.; Franke, V.; Lasagni, A.F. On the Ablation Behavior of Carbon Fiber-Reinforced Plastics during Laser Surface Treatment Using Pulsed Lasers. *Materials* **2020**, *13*, 5682. [CrossRef] [PubMed]
21. Fischer, F.; Kreling, S.; Dilger, K. Surface Structuring of CFRP by using Modern Excimer Laser Sources. *Phys. Procedia* **2012**, *39*, 154–160. [CrossRef]
22. Borengasser, M.; Hungate, W.S.; Watkins, R. *Hyperspectral Remote Sensing*; CRC Press: Boca Raton, FL, USA, 2007; ISBN 9781420012606.
23. Dale, L.M.; Thewis, A.; Boudry, C.; Rotar, I.; Dardenne, P.; Baeten, V.; Pierna, J.A.F. Hyperspectral Imaging Applications in Agriculture and Agro-Food Product Quality and Safety Control: A Review. *Appl. Spectrosc. Rev.* **2013**, *48*, 142–159. [CrossRef]
24. Calin, M.A.; Parasca, S.V.; Savastru, D.; Manea, D. Hyperspectral Imaging in the Medical Field: Present and Future. *Appl. Spectrosc. Rev.* **2014**, *49*, 435–447. [CrossRef]
25. Gendrin, C.; Roggo, Y.; Collet, C. Pharmaceutical applications of vibrational chemical imaging and chemometrics: A review. *J. Pharm. Biomed. Anal.* **2008**, *48*, 533–553. [CrossRef]
26. Gruber, F.; Grählert, W.; Wollmann, P.; Kaskel, S. Classification of Black Plastics Waste Using Fluorescence Imaging and Machine Learning. *Recycling* **2019**, *4*, 40. [CrossRef]
27. Gewali, U.B.; Monteiro, S.T.; Saber, E. Machine Learning Based Hyperspectral Image Analysis: A Survey. 2018. Available online: http://arxiv.org/pdf/1802.08701v2 (accessed on 14 April 2022).
28. Paoletti, M.E.; Haut, J.M.; Plaza, J.; Plaza, A. Deep learning classifiers for hyperspectral imaging: A review. *ISPRS J. Photogramm. Remote Sens.* **2019**, *158*, 279–317. [CrossRef]
29. Lu, G.; Fei, B. Medical hyperspectral imaging: A review. *J. Biomed. Opt.* **2014**, *19*, 10901. [CrossRef] [PubMed]
30. Lu, B.; Dao, P.; Liu, J.; He, Y.; Shang, J. Recent Advances of Hyperspectral Imaging Technology and Applications in Agriculture. *Remote Sens.* **2020**, *12*, 2659. [CrossRef]
31. Vater, J.M.; Gruber, F.; Grählert, W.; Schneider, S.; Knoll, A.C. Prediction of Coating Adhesion on Laser-Cleaned Metal Surfaces of Battery Cells Using Hyperspectral Imaging and Machine Learning. *Coatings* **2021**, *11*, 1388. [CrossRef]
32. Ronneberger, O.; Fischer, P.; Brox, T. U-Net: Convolutional Networks for Biomedical Image Segmentation. In *Medical Image Computing and Computer-Assisted Intervention—MICCAI 2015*; Navab, N., Hornegger, J., Wells, W.M., Frangi, A.F., Eds.; Springer International Publishing: Cham, Switzerland, 2015; pp. 234–241, ISBN 978-3-319-24573-7.
33. Gustke, K.; Gebauer, J.; Drehmann, R.; Lasagni, A.F.; Lampke, T. Enhancement of the Adhesion of Wire Arc Sprayed Coatings on Carbon Fiber-Reinforced Plastic by Surface Laser Structuring. *Coatings* **2021**, *11*, 467. [CrossRef]
34. Chollet, F. Xception: Deep learning with depthwise separable convolutions. In Proceedings of the IEEE Conference on Computer Vision and Pattern Recognition, Honolulu, HI, USA, 21–26 July 2017; pp. 1251–1258.
35. Li, L.; Jamieson, K.; DeSalvo, G.; Rostamizadeh, A.; Talwalkar, A. Hyperband: A Novel Bandit-Based Approach to Hyperparameter Optimization. *J. Mach. Learn. Res.* **2017**, *18*, 6765–6816.
36. François Chollet. *Keras*. 2015. Available online: https://keras.io/getting_started/faq/#how-should-i-cite-keras (accessed on 14 April 2022).
37. Tieleman, T.; Hinton, G. Lecture 6.5-rmsprop: Divide the gradient by a running average of its recent magnitude. *COURSERA: Neural Netw. Mach. Learn.* **2012**, *4*, 26–31.
38. Kingma, D.P.; Ba, J. Adam: A Method for Stochastic Optimization. 2014. Available online: http://arxiv.org/pdf/1412.6980v9 (accessed on 14 April 2022).